

1 **A 50% increase in the mass of terrestrial particles delivered by the Mackenzie River**
2 **into the Beaufort Sea (Canadian Arctic Ocean) over the last 10 years**

3

4 David Doxaran¹, Emmanuel Devred² and Marcel Babin²

5

6 *¹Laboratoire d'Océanographie de Villefranche, UMR 7093 CNRS-UPMC, Villefranche-sur-*
7 *Mer, France*

8 *²Takuvik Joint International Laboratory, CNRS - Université Laval, Québec, Canada*

9

10 *Correspondence to:* David Doxaran (doxaran@obs-vlfr.fr)

11

12

13 **Abstract**

14

15 Global warming has a significant impact at the regional scale on the Arctic Ocean and
16 surrounding coastal zones (i.e., Alaska, Canada, Greenland, Norway and Russia). The recent
17 increase in air temperature has resulted in increased precipitation along the drainage basins of
18 Arctic Rivers. It has also directly impacted land and seawater temperatures with the
19 consequence of melting the permafrost and sea-ice. An increase in freshwater discharge by
20 main Arctic rivers has been clearly identified in time series of field observations. The
21 freshwater discharge of the Mackenzie River has increased by 25% since 2003. This may
22 have increased the mobilization and transport of various dissolved and particulate substances,
23 including organic carbon, as well as their export to the ocean. The release from land to the
24 ocean of such organic material, which was sequestered as frozen since the last glacial
25 maximum, may significantly impact the Arctic Ocean carbon cycle as well as marine

26 ecosystems.

27 In this study we use 11 years of ocean-colour satellite data and field observations collected in
28 2009 to estimate the mass of terrestrial suspended solids and particulate organic carbon
29 delivered by the Mackenzie River into the Beaufort Sea (Arctic Ocean). Our results show that
30 during the summer period the concentration of suspended solids at the river mouth, in the
31 delta zone and in the river plume has increased by 46%, 71% and 33%, respectively, since
32 2003. Combined with the variations observed in the freshwater discharge, this corresponds to
33 a more than 50% increase in the particulate (terrestrial suspended particles and organic
34 carbon) export from the Mackenzie River into the Beaufort Sea.

35

36 **1. Introduction**

37

38 The Arctic Ocean plays an important role in the global carbon cycle as it contributes to up to
39 14% of the global ocean uptake of atmospheric carbon dioxide (Bates and Mathis, 2009).
40 Observations over the last 20 years have revealed significant impacts of climate change at
41 high latitudes, notably in the Arctic Ocean and surrounding coastal zones (Serreze et al. 2000,
42 Macdonald et al. 2006). Air temperature has increased by 1°C since 1980 (Overland et al.
43 2011). Precipitation over the drainage basin of the Arctic Ocean, the largest after the Atlantic
44 Ocean, has overall increased by 100 mm y⁻¹ since 2000 but with strong regional differences
45 (Rawlins et al. 2006). Consequently the freshwater discharge from major Arctic rivers has
46 also increased (e.g., Figure 1; Shiklomanov et al. 2007, Wisser et al. 2010, Shiklomanov and
47 Lammers 2011). Finally, the permafrost has been found to gradually thaw (Smith et al. 2005,
48 Zhang et al. 2012, Price et al. 2013). The permafrost is known to contain large amounts of
49 frozen organic matter sequestered since the last glacial maximum. The combination of
50 permafrost thawing and increase of Arctic rivers freshwater discharge (Li et al. 2009) may
51 lead to an increase in the flux of terrestrial substances delivered by rivers into the Arctic
52 Ocean.

53 More than ten years ago, Syvitski (2002) used a stochastic model to estimate the impact of
54 climate change (warming of Arctic regions) on sediment discharge by Arctic rivers. His study
55 predicted a 22% increase in the flux of sediment carried out by rivers for every 2°C warming
56 of the averaged drainage basin temperature and an increase of 10% in sediment load for a
57 20% increase in river discharge. Recent advancements in measuring capabilities may now
58 give us the possibility to confirm, or not, the realism of such predictions.

59 While field observations have been and are still scarce in such remote regions (e.g., along the
60 drainage basins of North American and Siberian rivers), a methodology has been recently

61 developed to remotely sense the variations of suspended particulate matter (SPM)
62 concentrations at the mouth of Arctic rivers using ocean colour radiometry (Doxaran et al.
63 2012). This method can be combined with field measurements of the river discharge and
64 particulate organic content to estimate the actual mass of terrigenous particles (suspended
65 particulate matter (SPM) and particulate organic carbon (POC)) supplied to the ocean by any
66 Arctic river and study its seasonal and interannual variations since ocean colour satellite data
67 are available for more than a decade (see for instance Doxaran et al., 2009).

68 The present study focuses on the mouth and turbid plume of the Mackenzie River in the
69 Beaufort Sea (Canadian Arctic Ocean). This river is the largest single source of terrestrial
70 particles entering the Arctic Ocean. The regional ocean colour algorithm developed by
71 Doxaran et al. (2012) for this area is based on a large bio-optical *in situ* dataset collected in
72 2009 during the MALINA oceanographic campaign. It has been successfully tested on a
73 selection of cloud-free and sea-ice-free ocean colour satellite images recorded during the
74 2009, 2010 and 2011 summer periods. It is here first improved to efficiently discriminate the
75 floating sea-ice, clouds, haze and highly turbid waters near the mouth of the Mackenzie River
76 by tuning processing flags and visually inspecting every single pass. It is then applied to an
77 11-year long dataset of ocean colour observations from the Moderate Resolution Imaging
78 Spectroradiometer (MODIS) onboard the Aqua satellite platform. Results are used to estimate
79 the monthly fluxes of SPM and terrestrial POC delivered by the Mackenzie River to the
80 Beaufort Sea during the melting season in order to reveal possible trends resulting from the
81 observed increase in freshwater discharge since 2003 (Figure 1). The evolution of the floating
82 sea-ice cover and extension of the Mackenzie River plume are also analyzed and discussed.

83

84 [Insert Figure 1 about here]

85

86 2. Data and methods

87

88 2.1 Study area

89

90 The southeast of the Beaufort Sea is characterized by the presence of a large and shallow
91 continental shelf bordered to the east by the Amundsen Gulf, to the west by the Mackenzie
92 canyon, to the south by the delta of the Mackenzie River, and to the north by the Beaufort Sea
93 and Canada Basin (Figure 2, Carmack and MacDonald, 2002). Two river mouths characterize
94 the shallow delta zone, one in the west side where both the river flow and water turbidity are
95 usually large and one in the east side with a low river flow. During the winter period, sea-ice
96 accumulates north of the delta zone resulting in the formation, along the 20 m isobath, of a
97 ridged ice barrier of considerable thickness (>20 m) grounded to the sea bottom, known as
98 stamukhi zone or stamukha (Macdonald et al., 1995). During that period, the water from the
99 Mackenzie River is trapped in the delta zone and forms what is essentially a lake of turbid
100 freshwater (Carmack and Macdonald, 2002). The spring ice break-up begins with the flooding
101 of the Mackenzie River. When the river flow is maximal (June) the turbid freshwaters
102 inundate the coastal zone and contribute to the progressive breaking of the stamukha (Figure
103 2). The warm and turbid river plume can then spread over an area of several thousand km²
104 to an offshore limit of permanent floating sea-ice (Macdonald et al., 1995). The extension and
105 dynamics of the plume are mainly controlled by wind conditions. During the summer period,
106 melting sea-ice and inputs from the Mackenzie River result in a 5 to 10 m surface layer of
107 freshwater over the continental shelf. In September, the shelf is usually completely free of
108 sea-ice up to around 72°N. Suspended particles supplied by the river are transported across
109 the continental shelf either in a surface plume or a benthic nepheloid layer. This transport is
110 controlled by circulation patterns on the shelf, which are driven by wind forcing, river

111 discharge and sea ice coverage (Ehn et al. submitted).

112

113 [Insert Figure 2 about here]

114

115 2.2 Satellite data and SPM algorithm

116

117 2.2.1 Ocean colour satellite data

118

119 As in Doxaran et al. (2012), the selected ocean colour satellite data are those recorded by the
120 MODIS (for Moderate Resolution Imaging Spectroradiometer) sensor onboard the Aqua
121 platform. This sensor provides every day at least one image of the study area since 2002 and
122 has several bands in the near-infrared (NIR) and short-wave infrared (SWIR) spectral regions
123 which are required for atmospheric corrections over turbid coastal waters (Wang and Shi,
124 2007). A single satellite sensor was used in this study in order to generate a consistent time
125 series of SPM concentration.

126 MODIS-Aqua level 1 data were downloaded from the National Aeronautics and Space

127 Administration (NASA) Ocean colour website (<http://oceancolor.gsfc.nasa.gov>) and

128 processed using the SeaWiFS Data Analysis System (SeaDAS 7.0.2) software

129 (<http://seadas.gsfc.nasa.gov/>). The 11-year time series spans from 2003 to 2013 and includes

130 the months of May to September, which correspond to the daylight period and ice-free season

131 in most of the Arctic Ocean. No data were available between October and April due to ice-

132 cover and the polar night; however, these missing data do not impact our results significantly.

133 In April, the river discharge is close to its annual minimum (reached in March, results not

134 shown) and sediment transport is low. In October, the river discharge is low and the onset of

135 the winter freeze-up reduces the export of sediment from the permafrost to the Mackenzie

136 River.

137 Removal of the atmospheric contribution to the total signal was performed using the NIR-

138 SWIR algorithm of Wang and Shi (2007); this correction method was proved to be the most

139 appropriate for the highly turbid waters (high SPM load) present in the mouth the Mackenzie

140 River (Doxaran et al. 2012). Due to high loads of SPM in the Mackenzie delta, a number of

141 marine pixels were often classified as clouds or ice-covered in the standard SeaDAS

142 processing (i.e., using the default mask threshold values) due to high reflectances values in the

143 near-infrared. This issue was tackled by increasing the cloud albedo threshold for cloud

144 flagging in the atmospheric correction procedure from the initial value of 0.027 to 0.4 in a

145 small area bounded eastwards from -133.4 to -138.9°E and northwards from 68.7 to 69.3°N

146 (Figure 2). Relaxation of the cloud albedo criteria was associated with a careful visual check

147 of every individual pass to avoid contamination by clouds in the delta, which occurred as

148 speckles of very high SPM concentrations. Finally, observations over the delta, when

149 available, were merged with the observation carried out with the standard atmospheric

150 correction scheme to obtain maps of the whole study area (Figure 3). The atmospheric

151 correction procedure yielded remote sensing reflectances, R_{RS} in sr^{-1} , at 555 and 748 nm,

152 which were used to derive the suspended particulate matter concentration (see next section).

153 Satellite products were generated at a spatial resolution of 1 km at nadir.

154

155 [Insert Figure 3 about here]

156

157 From an initial total of about ten thousands images downloaded over the study area between

158 2003 and 2013, and despite the large number of MODIS-Aqua revisits at high latitudes, only

159 562 images were finally exploited in the present study. This emphasizes the need for a

160 constellation of low-earth-orbit ocean colour satellites to increase the number of observations

161 in such areas, which are highly affected by clouds and sea ice. Due to the very high sea-ice
162 and cloud covers, the data recorded during the month of May finally proved to be unusable for
163 SPM retrieval and were discarded from our analysis. Interestingly, the number of images per
164 month increases with time along the observation period (2003-2013). This is consistent with
165 the receding of sea-ice concentration over the last decade. The highest number of images in a
166 month was reached in July 2012 (Figure 4), year of the record-low sea-ice extent (Perovich et
167 al. 2013). Whereas the minimum of sea-ice extent occurs in September (a usually very cloudy
168 month in this region), the highest number of satellite observations occurs in July when
169 daylight lasts more than twenty hours with higher sun zenith angles compared to the month of
170 September allowing a greater number of observations in July than in September. The number
171 of available images for each month was recorded to weight the linear regression of monthly
172 SPM concentration against time during time series analysis.

173

174 [Insert Figure 4 about here]

175

176 2.2.2 SPM algorithm and flux estimation

177

178 The suspended particulate matter (SPM) concentration varies over four orders of magnitude
179 (typically from 0.1 to more than 100 g m⁻³) from the highly turbid waters of the Mackenzie
180 delta to the oligotrophic region of the Beaufort Sea (e.g., Doxaran et al. 2012). At high SPM
181 concentration, the seawater reflectance signal tends to saturate in the visible part of the
182 spectrum and only the signal in the near-infrared (NIR) remains sensitive to SPM variations
183 (Doxaran et al. 2002, Shen et al. 2010). Therefore, as one of the main objectives of the study
184 was to quantify SPM concentration and estimate SPM flux at the mouth of the Mackenzie
185 River, a relationship had to be established between R_{RS} in the NIR and the SPM concentration.

186 Doxaran et al. (2012) established such a regional relationship, using the 748 nm (MODIS
 187 band 15) to 555 nm (MODIS band 4) remote sensing reflectance ratio, based on field bio-
 188 optical measurements carried out in the study area during the MALINA oceanographic
 189 campaign (in-water and above-water radiometric measurements were used to compute the R_{RS}
 190 signal; water samples were collected at 0.2 m depth using either a Niskin or a glass bottle for
 191 the determination of the SPM concentration (see Doxaran et al. 2012 for details)). This second
 192 order polynomial relationship is valid for a wide range of SPM concentrations spanning from
 193 1 to 150 g m^{-3} , i.e., valid from the mouth of the Mackenzie River up to the offshore limit of
 194 the river plume. This second order polynomial expression can accurately be described by two
 195 linear relationships: one developed for moderately turbid waters and a second one developed
 196 to deal with high concentration of SPM. To avoid a brutal change in the SPM concentration as
 197 a function of the $R_{RS}(748):R_{RS}(555)$ spectral band ratio, a non-linear equation (Eq. 1) was used
 198 to describe transition between both linear relationships:

199

$$\begin{aligned}
 200 \quad & \text{SPM} = 0.8386 \times R_{RS}(748:555) \quad \text{if } R_{RS}(748:555) < 87\% \\
 201 \quad & \text{SPM} = 70 + 0.1416 \times R_{RS}(748:555) + 2.9541 \times \exp[0.2092 \times (R_{RS}(748:555) - 87)] \quad \text{if } 87\% \leq R_{RS}(748:555) \leq 94\% \\
 202 \quad & \text{SPM} = 3.922 \times R_{RS}(748:555) - 285.4 \quad \text{if } 94\% < R_{RS}(748:555)
 \end{aligned}$$

203

204 Where SPM is the SPM concentration in g m^{-3} and $R_{RS}(748:555)$ is the ratio of remote sensing
 205 reflectance at 748 to 555 nm.

206 The use of two linear relationships is needed as the remote sensing reflectance signal in the
 207 NIR linearly increases with increasing SPM concentration up to about 90 g m^{-3} then starts to
 208 saturate at higher concentrations. Moreover, the sensitivity of the $R_{RS}(748)$ signal is lower and
 209 therefore not optimal in the lowest SPM range, namely 1 to 10 g m^{-3} , which corresponds to
 210 the offshore limit of the river plume. In that case, shorter wavelengths such as 555 nm (i.e.,
 211 the green part of the spectrum) are better suited (Nechad et al. 2010). As a consequence, our

212 regional algorithm is expected to accurately retrieve the SPM concentration in the delta zone
213 and map the extension of the river plume, but is potentially associated with higher
214 uncertainties in the retrieval of SPM concentrations in the less turbid waters of the river plume
215 (i.e., SPM lower than 10 g m^{-3}). To circumvent this issue, the Mackenzie plume was here
216 characterized by the water mass with surface SPM concentrations higher than 10 g m^{-3} , a
217 rather conservative threshold.

218 The semi-empirical relationship was established based on field measurements collected
219 during the 2009 summer period. It is assumed here to be valid for the entire period of satellite
220 observations (2003-2013). The uncertainty associated with the remotely sensed SPM
221 concentrations derived from our algorithm is estimated as $\pm 25\%$ based on (i) match-ups with
222 in situ data (when applying a similar SPM quantification algorithm to another study area: the
223 Gironde estuary, France (Doxaran et al. 2009)) and (ii) in situ measurements in the Mackenzie
224 delta zone (see Fig. 6 in Doxaran et al. 2012).

225 The SPM flux was computed each month, from June to September, simply by multiplying the
226 monthly-averaged SPM concentration (in g m^{-3}) by the monthly-averaged freshwater
227 discharged by the river (in $\text{m}^3 \text{ s}^{-1}$) for the same month and by the duration (in s) of each
228 month. This approach is simplistic but gives a robust estimate of average SPM fluxes in the
229 very shallow river mouth and delta zones. It does not require measurements of vertical
230 profiles of current velocities. The estimates were computed for two specific geographical
231 zones: (i) the river mouth defined as a box: $68.7^\circ\text{N} - 69.5^\circ\text{N}$ and $133^\circ\text{W} - 137^\circ\text{W}$ where the
232 offshore limit is about the 5-m isobath and (ii) the delta zone, also defined as a box: $68.7^\circ\text{N} -$
233 70°N and $132^\circ\text{W} - 139^\circ\text{W}$ where the offshore limit is about the 20-m isobath.

234

235 2.2.3 Sea-ice concentration

236 Satellite-derived sea-ice concentration, expressed in percentage (%), corresponds to the area

237 of a pixel covered by sea-ice relative to the total area of that pixel, such that a value of 100
238 indicates a pixel that is totally covered by sea-ice and a value of 0 indicates a pixel free of sea-
239 ice. It is computed using linear combination of the ratio of brightness temperatures measured
240 in the microwave spectrum using the NASA Team 2 algorithm (Markus and Cavalieri, 2000).
241 Daily sea-ice concentration data were downloaded from the ftp server of the Zentrum für
242 Marine und Atmosphärische Wissenschaften (ZMAW, ftp-projects.zmaw.de) between 2003
243 and 2013. A series of three sensors with a spatial resolution of 6.25 km was used to cover the
244 time period of MODIS-Aqua observations. From 2003 to 2011; data from the Advanced
245 Microwave Scanning Radiometer - Earth Observing System (AMSR-E) were used until it
246 stopped producing data. The new satellite AMSR2, launched in January 2013, was used to
247 estimate the sea-ice concentrations in 2013. The gap between the AMSR-E and AMSR2
248 sensors (2012) was filled using data from the Special Sensor Microwave Imager/Sounder
249 (SSMIS). Sea-ice concentration was used to flag potentially contaminated water pixels
250 (isolated water pixels surrounded by highly reflective sea-ice sometimes present erroneous
251 high reflectance values due to adjacency effects). In that respect, ocean colour data collected
252 over pixels with a sea-ice concentration greater than 10% were removed from our analysis
253 following Bélanger et al. (2007). The data were also used in time series analysis to obtain
254 information on the variations of sea-ice cover over time in the region of interest.

255

256 2.2.4 Daily observations of SPM and sea-ice concentrations

257

258 Figure 5 illustrates the resulting observations made on each individual MODIS satellite image
259 when combined to the daily mapped sea-ice concentration data. This example shows the
260 spectacular spring ice break-up event (typically occurring in early or mid-June) and highlights
261 the rapid stamukha breakdown, which allows the turbid freshwaters of the Mackenzie River

262 initially constrained in the delta zone to spread over the Beaufort shelf. Figure 5 also
263 highlights the contrast between the spring and the mid-summer period (early August) when,
264 during the latest, the coastal zone is totally free of ice. On June 12 in 2004, a wide ice barrier
265 extends all along the coast with sea-ice concentrations still close to 100% in the Mackenzie
266 delta zone, in the Amundsen Gulf and over most of the open ocean waters of the Beaufort
267 Sea. Note that SPM concentrations in the ice-free waters (between the stamukha and floating
268 sea-ice) are already high (about 10 g m^{-3}) as turbid plumes can spread out in the continental
269 shelf from below the stamucha (e.g., see Figure 2 for illustration). Not surprisingly, a week
270 later (on June 19), the breaking of the stamukha occurs first right in front of the Mackenzie
271 River mouth (west side) where the river flow is maximum. The turbid plume clearly remains
272 up to the offshore sea-ice edge, with SPM concentrations greater than 10 g m^{-3} . Two weeks
273 later, on June 28, the sea-ice concentration along the coast has significantly decreased and the
274 highest SPM concentrations (up to 100 g m^{-3}) are located in the delta zone. The extension of
275 the turbid plume has declined: the main direction of the plume closely follows the bathymetry
276 towards the Mackenzie canyon while clear waters appear around the plume. Finally, one
277 month and a half later (August 5), during the mid-summer period, the sea ice has almost
278 disappeared along the coast and notably at the entrance of the Amundsen Gulf. Offshore the
279 sea-ice remains but has retreated northwards following its seasonal cycle. The extension of
280 the river plume reaches its maximum size with highly turbid waters at the river mouth and in
281 the delta zone contrasting with clear waters offshore.

282 These four daily snap-shots provide an initial overview of the SPM and sea-ice seasonal
283 dynamics over the study area. However, performing a multi-year and seasonal analysis of
284 these two parameters requires the use of monthly-averaged composites.

285

286 [Insert Figure 5 about here]

287
288
289
290
291
292
293
294
295
296
297
298
299
300
301
302
303
304
305
306
307
308
309
310
311

2.2.5 Monthly compositing and time series analysis

Two main areas of interest are distinguished in the present study: (i) the river delta, as defined in Figure 2 and (ii) the river plume defined as the area where SPM was greater than 10 g m^{-3} .

Whereas the delta surface area remains constant in time, the surface area of the plume changes as a function of the SPM concentration dynamics over the shelf of the Beaufort Sea in turn driven by the river discharge, wind and sea-ice cover conditions. Monthly gridded images were computed on a pixel-per-pixel basis using the arithmetic mean of all the measurements available in a given month. The monthly mean SPM concentrations for the Mackenzie delta and plume (i.e., one value per month) were computed also by arithmetic mean within the area of interest, and the number of pixels used to compute each mean was recorded (N_{month}).

The limited number of months with conditions suitable for ocean colour observations due to ice cover and the polar night (i.e., about 4 months a year) prevents the use of common time series decomposition tools since it is not possible to obtain an entire annual cycle. We therefore preferred to use linear regressions of each satellite product (SPM, sea-ice concentration) against time to infer its trend. When performing the linear regression of monthly SPM concentration against time, the number of pixels available for each month, i.e. N_{month} , was used to weight the contribution of each month in the time series, and give more importance to month with more data. The time series analysis was carried out from 2003 to 2013 (11 years) from the month of June to the month of September.

3. Results

312 3.1 Seasonal dynamics of sea-ice and suspended particulate matter

313

314 We first look at the ‘seasonal’ dynamics of SPM and sea-ice in the region of interest. Here,
315 the term ‘seasonal’ refers to the monthly variations over the four months period (June to
316 September) which corresponds to the maximal Mackenzie River discharge (Figure 1). Also
317 before analyzing the multi-year variations and potential trends, we highlight how different can
318 be successive years in terms of sea-ice coverage and SPM dynamics.

319 Similar situations were observed in 2003 and 2004: in June, the ice extends all along the coast
320 except in front of the west branch of the Mackenzie River mouth (Figure 6). The water is
321 highly turbid in the delta zone and also on the continental shelf bounded in the north by the
322 offshore sea ice edge ($\sim 70.2^\circ\text{N}$) and in the east by the entrance of the Amundsen Gulf. One
323 month later, in July, the coast is free of ice while the floating sea ice still covers the same area
324 in the Beaufort Sea; a maximum turbidity zone has developed in the delta zone with SPM
325 concentrations up to 100 g m^{-3} and the turbid plume still extends from the river mouth up to
326 the offshore limit of sea ice. Progressively, in August then September, the extent and
327 concentration of floating sea ice both decrease as the concentration of SPM on the continental
328 shelf and in the delta zone.

329

330 [Insert Figure 6 about here]

331

332 The situation is much more peculiar in June 2006 as the whole Beaufort Sea is covered by
333 sea-ice except along the coastline and in the Mackenzie delta. These unusual June conditions
334 return to the average conditions in July as the floating sea ice has moved northwards:
335 extremely turbid waters then concentrate in the delta zone while turbid plumes extend along
336 the continental shelf. Once again in August and September SPM concentrations progressively

337 decrease on the shelf while remaining high in the delta zone. Opposite conditions are
338 observed at the beginning of the 2008 summer period with a minimum floating sea ice cover
339 observed from June to September (Figure 7). SPM concentrations gradually decrease along
340 the shelf during this period while remaining very high in the delta zone.

341

342 [Insert Figure 7 about here]

343

344 A high number of cloud-free days in 2011, 2012 then 2013 (Figure 4) yield a maximum of
345 satellite observations (Figure 8). In 2011, the stamukha zone can still be observed in June as it
346 progressively breaks, resulting in the presence of floating sea ice along the coast. High SPM
347 concentrations extend from the delta zone to the continental shelf with the main river plume
348 extending towards the Mackenzie canyon. In August and September, high SPM
349 concentrations are only detected in the delta zone while clear waters cover most of the
350 continental shelf. The minimum sea-ice cover is observed during the 2012 summer period,
351 allowing turbid plumes with high SPM concentrations to extend up to 72.5°N. Despite these
352 favorable sea-ice and cloud cover conditions, the monthly variations of SPM from June to
353 September remain similar to the monthly variations during the previous years. Finally,
354 opposite conditions to 2012 and 2011 are encountered in 2013 with sea ice covering most of
355 the Beaufort Sea in June, as in 2006, with only the delta zone being free of ice. As the floating
356 sea ice slowly migrates north from July to September, the discharge of the Mackenzie
357 freshwaters occurs later such that turbid waters extend over the continental shelf until August.
358 The situation in September is finally similar to the previous years, with high SPM
359 concentrations constrained to the delta zone and clear waters offshore.

360

361 [Insert Figure 8 about here]

362

363 3.2 Multi-year dynamics of sea-ice and SPM

364

365 The month of June is probably the most interesting to consider regarding the extent of sea ice
366 in the Beaufort Sea. The sea-ice cover depends primarily on the atmospheric conditions (air
367 temperature and wind) during the long winter period when ice has formed and extended south
368 from the very high latitudes (greater than 80°N). Close to the shore, the sea-ice cover also
369 depends on the air temperature and wind conditions along the coast, which determine the sea-
370 ice concentrations and thickness of the *stamukha*. Sea-ice is also affected by the heat content
371 of the underlying ocean, which varies from year to year, including because of changes in large
372 scale circulation. Finally, the June sea-ice extent is influenced by the freshwater discharge of
373 the Mackenzie River during the spring period (April, May and June), which defines the
374 upstream pressure imposed by the river to the ice barrier formed around the delta zone and
375 controls its breaking.

376 In June 2003, 2004 and 2005 similar conditions of sea ice and *stamukha* extents were
377 observed, with (i) floating sea-ice spreading over most of the Beaufort Sea south up to 70.5°N
378 and (ii) ice formed all along the coast up to the Amundsen Gulf. High SPM concentrations
379 were then located in the delta zone while turbid plumes were extending up to the offshore
380 limit of the sea ice. The following summer periods (July to September 2003 to 2005) also
381 showed similar patterns with a gradual regression of sea ice moving northwards and a decline
382 in the SPM load and offshore extension of the turbid plumes, which were progressively
383 constrained to the coast (delta zone). The years following 2005, i.e. 2006 to 2013 showed
384 more pronounced monthly variations with very different situations encountered in June, such
385 as an almost full coverage of the Beaufort Sea with sea-ice in 2006 and 2013, and quasi ice-
386 free conditions over the whole Beaufort Sea (up to 72.5°N) in 2012. Between these two

387 extreme situations (i.e. from full to null sea-ice coverage conditions in June), transition years
388 (e.g., 2007, 2008 and 2009) showed intermediate sea-ice conditions but on average the sea-ice
389 extent over the Beaufort Sea in June significantly decreased from the 2003-2005 period to the
390 most recent years. SPM dynamics over the summer period showed rather similar successive
391 patterns during the last 11 years: first the discharge of the highly turbid waters of the
392 Mackenzie River trapped in the stamukha, then the offshore transport of SPM mainly towards
393 the Mackenzie canyon and finally at the end of the summer period the trapping of SPM in the
394 delta zone in contrast to clear waters (low SPM loads) over the Mackenzie shelf.
395 It should be also noted that the number of MODIS-Aqua satellite observations over the study
396 area, so the number of cloud-free and sea-ice-free days, significantly increased from 2003 to
397 2013. Therefore before examining in detail the variations of SPM concentrations over this 11
398 years period, our analyses already reveal significant changes in both the sea ice and cloud
399 covers in the Beaufort Sea region.

400

401 3.3 Multi-year SPM concentrations and fluxes at the Mackenzie River mouth

402

403 The freshwater discharge of the Mackenzie River (data for the station 10LC014 (67° 27' 21"
404 N and 133° 45' 11" W) from 1972 to 2013 were downloaded from the Environment Canada
405 website (www.wateroffice.ec.gc.ca). It shows large seasonal variations (Figure 1) with a
406 maximum during the summer period (from June to September) and lower values during the
407 rest of the year (Macdonald et al., 1995, O'Brien et al., 2006). Over the last 11 years, this
408 discharge typically varied between 4000 m³ s⁻¹ (winter) and 25 000 m³ s⁻¹ (summer). Despite
409 large year-to-year variations, a trend is found over this period with a significant increase of
410 22% from 2003 to 2013.

411 The analysis of the monthly SPM maps generated from 2003 to 2011 provides a qualitative

412 overview of the spatial and temporal variations of SPM concentrations in the Mackenzie
413 mouth and delta, as well as in the Beaufort Sea. In order to quantify these variations and
414 highlight a potential trend, these monthly-averaged SPM concentrations were plotted as a
415 function of time, first only considering the Mackenzie delta zone (see Figure 2 for detailed
416 geographical location).

417 For the 11 years of the time series, the four monthly-averaged SPM concentrations (June to
418 September) revealed the SPM variations during the summer period (i.e., when the Mackenzie
419 River mouth is directly connected to the Beaufort Sea), which gives a first overview of the
420 load of SPM exported from the river to the coastal ocean (Figure 9). These SPM
421 concentrations vary from about 70 g m^{-3} to 100 g m^{-3} during the 11 years period, which is in
422 agreement with field measurements collected along river transects (Doxaran et al. 2012). On
423 average over a selected summer period, relative variations of $\pm 25\%$ are retrieved, except in
424 2003 when relative variations of $\pm 65\%$ occurred. Note that the results obtained in 2003 may
425 be associated to larger uncertainties due to the relative low number of cloud-free satellite
426 images available. The highest SPM concentration over a summer period in the Mackenzie
427 delta is usually, but not systematically, observed in June or July (e.g., in 2013 when a high
428 number of cloud-free MODIS images were available). Despite these month-to-month
429 variations, a striking result lies in the multi-year trend observed during our 11 years
430 observation, which overall corresponds to an increase of the mean SPM concentration in the
431 delta zone from 2003 to 2013. Over this 11-year period, the mean concentration has increased
432 from 71 g m^{-3} to 107 g m^{-3} , which represents a significant increase of 51% since 2003. This
433 linear increasing trend is obvious ($R^2 = 0.61$) when considering the mean SPM concentration
434 averaged each year over the four-month observation time window (June to September). Such
435 an increase of more than 50% observed over the 11-year period is much higher than the
436 uncertainty of the SPM concentration estimated from MODIS satellite data using our

437 algorithm (+/-25% according to Doxaran et al. 2009, 2012), uncertainty which is significantly
438 minimized when producing monthly averages of SPM concentrations (assuming there is no
439 correlation between SPM and clouds). Moreover due to regular vicarious calibrations of the
440 MODIS-Aqua sensor (Franz et al. 2007, Meister et al. 2012), a temporal degradation in the
441 satellite data quality cannot explain the variations observed. This tends to confirm the
442 consistency of the result presented here. It is also important to remember that a unique
443 satellite sensor was used in this study and the exact same algorithm (atmospheric corrections
444 of satellite data and inversion of the seawater signal into SPM concentration) was applied,
445 precisely in order to avoid any bias or discrepancy related to sensor calibration and minimize
446 the uncertainty of the satellite-derived SPM concentration. This gives us confidence in the
447 validity of the increasing trend in monthly SPM concentration observed over the Mackenzie
448 River delta and Beaufort Sea.

449 To further confirm this assumption, we examine the relationship between the monthly-
450 averaged (i) Mackenzie freshwater discharge (in $\text{m}^3 \text{s}^{-1}$) and (ii) SPM concentration in the
451 delta zone. A correlation can be expected between the two variables which both increased, by
452 22% and 51% respectively, from 2003 to 2013. However, SPM concentration correlated with
453 freshwater discharge ($R^2=0.71$, $p\text{-value} < 0.05$) when considering only the months of May (1
454 point) and June (11 points), whereas no correlation ($R^2 = 0.07$) was established when all the
455 months (May to September) were accounted for (Figure 9b). This suggests that the export of
456 SPM from the Mackenzie River to the Beaufort Sea is largely driven by the Mackenzie River
457 runoff during a short period of two months (May and June, i.e., late spring and early summer)
458 corresponding to the maximum freshwater flow. Other mechanisms and processes may be
459 involved during the other summer months, such as permafrost thawing, intense precipitation
460 events that locally inject pulses of SPM in the Mackenzie River and delta which is later
461 exported to the Beaufort Shelf. In spring (May and June) the SPM simply goes through the

462 delta zone to enter the coastal ocean (the spring freshet is often the period of most flux in
463 many rivers as the velocities are sufficient to keep particles in suspension). As soon as the
464 river freshwater discharge decreases (July to September), the SPM is trapped in the delta zone
465 where particle settling and resuspension due to tidal currents and wind stress will control the
466 variations of SPM concentrations and export towards the continental shelf.

467

468 [Insert Figure 9 about here]

469

470 Having observed and quantified the increase of the Mackenzie freshwater discharge and SPM
471 concentration at the river mouth, the next logical step is to look at the resulting variation in
472 the SPM flux delivered by the river to the Arctic Ocean. The result is an estimation of the
473 mass of SPM in grams (g) transported downstream through the river mouth. The SPM flux
474 obtained corresponds to the solid discharge of the Mackenzie River into the Beaufort Sea, i.e.,
475 the mass of SPM delivered by the river each month during the June to September summer
476 period. The same SPM flux calculation is made in the delta zone but cannot be considered as
477 a horizontal downstream transport as this zone is also affected by SPM vertical dynamics
478 (particle settling and resuspension of bottom sediments). Note that here we call river mouth
479 the downstream limit of the Mackenzie River, i.e., the geographical zone defined as the box:
480 68.7°N – 69.5°N and 133°W – 137°W. The delta zone is the geographical zone defined as the
481 box: 68.7°N – 70°N and 132°W – 139°W.

482 The results obtained in the river mouth emphasize the large monthly variations in the SPM
483 flux (a factor of 6) during the summer period (Figure10a). The SPM flux is typically higher in
484 June and July than in August and September, which can be explained by the variations of the
485 Mackenzie River freshwater discharge. A strong interannual variability in the SPM flux is
486 also observed, which is directly related to the interannual variability in the freshwater

487 discharge. The timing of the break-up of the stamukha probably plays an important role in the
488 interannual variability of the SPM flux by slowing down the river flow into the delta zone. As
489 for the SPM concentrations (Figure 9), a trend of increasing SPM flux is observed from 2003
490 to 2013. Fitting this time series using a linear regression reveals a significant positive trend
491 (p -value < 0.05) with a relative slope of 46% increase over the 11-year long period of
492 observation. This result corresponds to about twice the increase observed in the river
493 freshwater discharge (Figure 1). Such an increase in the SPM flux may reflect enhanced
494 erosion processes occurring along the drainage basin as a result of the warming air
495 temperature and perhaps an acceleration of the thawing of the permafrost.

496 Similar observations are made in the delta zone (Figure 10b). It is interesting to note that the
497 SPM fluxes in the delta zone and at the river mouth are linearly correlated ($R^2 = 0.81$) with
498 SPM concentrations and SPM fluxes in the delta zone being approximately 30% lower. This
499 clearly indicates that rapid and intensive settling of particles occurs in the delta zone (e.g.,
500 Rontani et al. 2014). A second interesting observation is that the increase in SPM
501 concentrations and therefore in the resulting SPM flux from 2003 to 2013 is higher in the
502 delta zone (+71%) than in the river mouth (+46%). This certainly reflects an increase in water
503 turbidity, i.e., in SPM load, in the delta zone where particles rapidly settle to form a bottom
504 nepheloid layer and/or deposit. Resuspension processes due to tidal currents and wind stress
505 probably contribute in a non-negligible manner to the higher SPM concentrations observed in
506 this very shallow (2 to 5 meters depths) zone, however, our method does not allow the
507 separation of the different processes involved in the characterization of the SPM fluxes. When
508 considering the SPM fluxes each year averaged over the whole summer period, a linear fit is
509 obtained with a significant correlation ($R^2 = 0.43$) at the river mouth (Figure 10c). Note
510 however two peculiar years (2004 and 2010) associated to lower than expected SPM fluxes.
511 This relationship may be useful to model and predict in the near-future mass of SPM and

512 associated organic carbon delivered by the Mackenzie River into the Beaufort Sea. Using this
513 interannual linear trend, a significantly lower increase in SPM flux is obtained from 2003 to
514 2013: +36% instead of +46% when considering the monthly-averaged SPM fluxes (Figure
515 10a). This clearly means that the method used to estimate the changes in SPM concentrations
516 and fluxes impacts the result. While we can confidently conclude on the positive trends
517 observed in the SPM concentration and fluxes, the magnitude of the variations reported here
518 should be carefully used in other studies.

519

520 [Insert Figure 10 about here]

521

522 3.4 Impact on the Mackenzie continental shelf

523

524 We finally analyze the impact of the increase in SPM concentrations and fluxes in the river
525 mouth and delta zone on the Mackenzie continental shelf (Figure 11). Only the SPM
526 concentrations (estimated using satellite data within the first few meters below the air-water
527 interface (Doxaran et al. 2012)) are considered here. Given the data available in this study, it
528 is impossible to compute the SPM flux as we do not have access to the surface current
529 velocity and direction. The extent of the plume over the study area is defined as the area
530 where SPM concentrations are higher than 10 g m^{-3} . This arbitrary threshold value was chosen
531 because of the higher accuracy of our remote sensing algorithm in the 10 to 100 g m^{-3} SPM
532 concentration range. The resulting mean SPM concentration in the river plume is logically
533 lower than in the delta zone. They typically vary from 40 to 80 g m^{-3} (with few values as low
534 as 20 g m^{-3}) (Figure 11a), compared to variations from 60 to 120 g m^{-3} in the delta zone
535 (Figure 8). This simply highlights the balance between horizontal transport of SPM within
536 surface waters and settling within the water column, as well as degradation processes (see

537 details in Rontani et al. 2014). Monthly variations of SPM concentrations in the river plume
538 are slightly smoother than in the river mouth and delta zone, probably due to the large surface
539 covered by the plume. A very similar trend of increasing concentrations is observed along the
540 11-year period (+33%). The turbidity of the water along the Mackenzie continental shelf is
541 also rising and this certainly will have a direct impact on the marine ecosystems, since it will
542 modify the nutrient balance (possible increase in primary production) but also will reduce the
543 light availability within the water column (decrease in primary production) (see Forest et al.
544 2013 for detailed analyzes). Increasing volumes of turbid freshwater delivered into the
545 Mackenzie continental shelf will also impact on the stratification of water masses (e.g.,
546 buoyancy of surface waters) and alter primary production.

547 The extent of the Mackenzie River plume mainly experienced strong month-to-month
548 variations, being typically at a maximum in June then progressively decreasing until August
549 and September. This clearly reflects the observations made on the SPM maps (Figures 6 to 8):
550 the river plume spreads out over the shelf during the break-up of the stamukha and regresses
551 to the coast, mainly in the delta zone, during the summer period as the river discharge and
552 thus freshwater transport decrease. There is no significant interannual trend observed
553 concerning the plume extent as it is mainly dependent on the sea-ice coverage and the
554 regional hydrodynamic (Ehn et al. submitted). While SPM concentrations increase within the
555 surface waters of the plume, its extension in the Beaufort Sea remains unchanged due to the
556 presence of the pack of floating sea ice. A direct impact of the decrease in sea-ice extent has
557 been observed on primary productivity of Arctic waters (Arrigo et al. 2008, Tremblay et al.
558 2011). However, it is not understood yet whether this increase in terrestrial substances along
559 the continental shelf contribute to the development of phytoplankton blooms under the Arctic
560 sea ice (Arrigo et al. 2012).

561

562 [Insert Figure 11 about here]

563

564 **4. Discussion**

565 An important result presented in the previous section concerns the significant increase of SPM
566 flux at the mouth of the Mackenzie River observed over the last 11 years, with potential effect
567 not only on the marine ecosystem but also on the northern community. Erosion of the
568 shoreline has dramatic consequences for the local community and an increase in sediment
569 transport and deposit along the Beaufort shelf could mitigate the impact of the erosion.

570 However, numerical model of ocean circulation would be required to properly assess the fate
571 of the extra sediment exported. Another important aspect of our findings concerns the mass of
572 terrestrial SPM (and subsequent POC) exported from the Mackenzie River to the Beaufort Sea
573 and to balance this budget with the sedimentation rates in the delta zone and continental shelf.
574 Taking into account the degradation process of the organic material within the water column
575 (Bélanger et al. 2006) and the fate of bottom sediments (Chaillou et al. 2007), it is necessary
576 to quantify the percentage of terrestrial organic matter that will be buried into marine
577 sediments and attempt to explain it by taking into account the highly refractory state of POC
578 transported by rivers (Hedges et al. 1997, Keil et al. 1997).

579 At the mouth of the Mackenzie River, water masses are transported downstream to enter the
580 delta zone to supply it with dissolved and particulate materials. As a first approximation, the
581 SPM flux estimated in the present study corresponds to the mass of SPM delivered by the
582 river to the delta during the four-month summer period (June to September). On average from
583 2003 to 2013, the total mass of SPM estimated during this period is about $20 (\pm 5) \times 10^{12} \text{ g a}^{-1}$,
584 which is in good agreement with previous estimates made using a selection of cloud-free
585 satellite images recorded in 2009, 2010 and 2011 (Doxaran et al. 2012). Assuming a constant
586 POC:SPM organic content of 1.8% (mean value reported by Yunker et al. 1993, Emmerton et

587 al. 2008 and Doxaran et al. 2012, while values as low as 1.1% and as high as 3.4% have been
588 observed in the river mouth area during the June-September period), this leads to a total of 0.4
589 $(\pm 0.1) \times 10^{12}$ gC a⁻¹ of terrestrial POC entering the delta zone through the Mackenzie River
590 mouth. These values must be compared to previous estimates made based on field
591 measurements (freshwater discharge and sediment loads) collected in the Mackenzie River
592 hundreds of kilometers upstream the delta zone (Macdonald et al. 1998): $120 (\pm 5) \times 10^{12}$ g a⁻¹
593 for SPM and $2.0 (\pm 0.5) \times 10^{12}$ gC a⁻¹ for POC. There are several reasons to explain such
594 differences (factor 5 to 6) on SPM and POC estimated in our study and those reported in
595 Macdonald et al. (1998). First, the satellite observations used in the present study cover only
596 four months over the year, i.e. June to September, a period during which occurs about 50% of
597 the freshwater discharge (McClelland et al. 2012). Assuming a constant SPM concentration in
598 the river along the year, extrapolating our results to the winter period would lead to total of 40
599 $(\pm 5) \times 10^{12}$ g a⁻¹ for SPM, i.e., still a factor 3 difference with the delivery estimated by
600 Macdonald et al. (1998). As the organic SPM content is higher during the winter (being 5%
601 instead of 2% during the summer period (Yunker et al. 1993), our summer estimates can be
602 extrapolated to $1.3 (\pm 0.1) \times 10^{12}$ gC for the annual POC delivery into the delta which still
603 represents a 50% difference with Macdonald et al. (1998) estimates.

604 It is important to attempt to explain such differences. On one hand, estimates based on field
605 measurements by Macdonald et al. (1998) relied on data collected at least 100 km upstream of
606 the delta zone (i.e., at the Arctic Red River station). The complex network of secondary
607 streams branching out of the river in the upper Mackenzie delta may act as an efficient
608 trapping for SPM, which would imply that an annual delivery of 120×10^{12} g into the delta
609 zone is overestimated. This would correspond to mean depth-averaged SPM concentration in
610 the order of 500 g m^{-3} at the river mouth all along the year, which is typically more than twice
611 the values actually observed in the field during the MALINA oceanographic campaign and

612 also significantly higher than SPM concentrations remotely sensed using MODIS satellite
613 data (Doxaran et al. 2012). On the other hand ocean colour satellite observations are very
614 scarce at best and therefore not exploitable in April and May, two months usually associated
615 to high river runoff and break-up of the stamukha, thus potentially associated to a maximum
616 solid discharge into the delta. Moreover, the mean SPM concentrations obtained from satellite
617 data slightly vary depending on the limits of the geographical zone in which the averaged is
618 computed as fine particles in suspension in the river freshwaters rapidly form flocs or
619 aggregates as soon the water salinity becomes positive (Eisma et al. 1991). Therefore
620 suspended particles rapidly settle when they enter the delta zone, which leads to lower
621 concentration within the upper layer of the water column measured by the ocean color sensor.
622 Finally, satellite observations measure only the SPM concentration in the first meter (if not
623 less) below the air-water interface due to the rapid attenuation of the radiative signal, such
624 that the presence of a bottom nepheloid layer (BNL) cannot be detected. The BNL is usually
625 present at the downstream limit of the delta (Doxaran et al. 2012) and along the inner
626 continental shelf (Ehn et al. submitted) and could play an important role in the SPM export
627 from the river to the delta. In such a case the SPM fluxes estimated using satellite data would
628 provide an underestimation of the actual SPM loads delivered by the river to the delta. The
629 true annual discharge of SPM by the Mackenzie River into the Beaufort Sea is probably in
630 between 40 and 120×10^{12} g. Only high frequency measurements aboard *in situ* autonomous
631 platforms installed at the mouth of the Mackenzie River and equipped with several turbidity
632 sensors from the bottom (to sample the BNL) to the surface (to calibrate satellite data),
633 together with detailed observations of current velocity profiles along and across the river
634 mouth, could provide the information needed to conclude and accurately compute the SPM
635 fluxes exported by the Mackenzie River.

636

637 **5. Conclusions and perspectives**

638

639 For the first time to our knowledge, ocean colour satellite data at moderate spatial resolution
640 (1 km) have been routinely processed over the recent 11-years long period (2003-2013) to
641 estimate and map the SPM concentrations at the mouth and along the plume of the Mackenzie
642 River, in the Canadian Arctic Ocean. The regional algorithm developed by Doxaran et al.
643 (2012) initially applied to selected cloud-free MODIS scenes in 2009, 2010 and 2011 was
644 here optimized to minimize the effects of sea-ice, cloud and haze masks while also retrieving
645 the seawater reflectance over the highly turbid waters of the Mackenzie delta zone. This
646 improved algorithm was applied to MODIS-Aqua satellite data to extract a maximum of
647 information on SPM dynamics in the study area. As a result SPM maps were produced each
648 year from the beginning of June to the end of September, the remaining months were
649 discarded due to a lack of observations, a result of the combined effect of low solar light and
650 sea-ice covering most of the study area. It was interesting to note that probably due to effects
651 of climate change on the receding of sea-ice extent at high latitudes, a significant increase in
652 the number of images with valid pixels was recorded in May and October after 2010. Lastly,
653 sea-ice cover and SPM concentrations were superimposed to discard ocean colour data
654 possibly contaminated by the presence of sea-ice and to study the combined dynamics of sea
655 ice and SPM over the study area.

656 The monthly-averaged SPM and sea-ice maps produced were used to analyze the 'seasonal' to
657 interannual dynamics of SPM at the river mouth, in the delta zone and in the river plume. The
658 highest SPM concentrations and largest extension of the plume were systematically observed
659 in June, following the break-up of the stamukha and usually corresponding to the annual peak
660 of the river freshwater discharge. As the river flow progressively declined in August and
661 September, SPM concentrations gradually decreased in offshore waters but remained high in

662 and around the delta zone where SPM did accumulate. This probably results from other
663 processes involved in the transport of SPM, such as erosion due to permafrost thawing or
664 extreme rain events. In addition to strong interannual variations, a trend was observed in both
665 the delta zone and river plume, respectively corresponding to 50 and 35 (± 5) % increases in
666 the SPM concentrations. Combined with the simultaneous augmentation of the Mackenzie
667 River freshwater discharge over the same period (+22%), the resulting SPM flux estimated at
668 the river mouth significantly increased from 2003 to 2013 (+46%) probably due to enhanced
669 erosion processes along the drainage basin of the river. While in the same order of magnitude,
670 the total masses of SPM (and terrestrial POC) exported by the Mackenzie River into the
671 Beaufort Sea estimated using field measurements (Macdonald et al. 1998) and satellite data
672 (our study) are significantly different, the latter being lower. The combined use of field and
673 remote sensing techniques will be necessary in order to minimize the uncertainties associated
674 with these estimations. These results are in agreement with the modeling study of Syvitski
675 (2002), who predicted an increase of 20% of sediment load for every increase in 10% of
676 Arctic river discharge. In our case, we found an increase of 46% of SPM concentration in the
677 Mackenzie River delta for an increase of 22% in the freshwater river discharge. In a future
678 study, the use of high spatial resolution ocean colour satellite data (e.g., MODIS bands 1 and
679 2 respectively centered at 645 and 859, spatial resolution: 250 m) should allow us better
680 understanding the dynamics and transport of suspended particles at the river mouth
681 (discriminating the West and East river mouths) and in the delta zone, especially during the
682 breaking of the stamukha.

683 The observed increase in the river discharge of SPM and turbidity (SPM concentrations),
684 combined with changes in other key environmental factors in the coastal Arctic Ocean
685 (Tremblay et al. 2011), will certainly have a rapid impact on the fate of the terrestrial organic
686 carbon and on the marine ecosystems: ocean colour satellite observations have already

687 suggested an increase in the annual primary production in the Arctic Ocean (Arrigo et al.,
688 2008).

689

690 **6. Author contribution**

691

692 D. Doxaran actively contributed to in situ bio-optical measurements in the study area,
693 designed the regional SPM algorithm used in this study; he also contributed to its routine
694 application to ocean colour satellite data. E. Devred downloaded and processed the full time-
695 series of ocean colour satellite observations and analyzed the trends observed in the variations
696 of SPM concentrations and fluxes. M. Babin is at the origin of the whole study and was the
697 P.I. of the MALINA project (and oceanographic campaign). D. Doxaran prepared the
698 manuscript with contributions from all co-authors.

699

700 **7. Acknowledgements**

701

702 This study was funded by ANR, the French Agence Nationale de la Recherche (MALINA
703 project, P. I. M. Babin). We acknowledge the NASA GSFC for providing free access to
704 MODIS satellite data and SeaDAS software, Environment Canada, namely the Water Office
705 www.wateroffice.ec.gc.ca, for providing the daily water discharge of the Mackenzie River
706 main tributaries.

707 **References**

708

709 Arrigo, K. R., van Dijken, G., and Pabi, S.: Impact of a shrinking Arctic ice cover on marine
710 primary production, *Geophys. Res. Lett.*, 35, 10.1029/2008GL035028, 2008.

711 Arrigo, K. R., D. K. Perovich, R. S. Pickart, Z. W. Brown, G. L. van Dijken, K. E. Lowry, M.
712 M. Mills, M. A. Palmer, W. M. Balch, F. Bahr, N. R. Bates, C. Benitez-Nelson, B. Bowler, E.
713 Brownlee, J. K. Ehn, K. E. Frey, R. Garley, S. R. Laney, L. Lubelczyk, J. Mathis, A.

714 Matsuoka, B. G. Mitchell, G. W. K. Moore, E. Ortega-Retuerta, S. Pal, C. M. Polashenski, R.
715 A. Reynolds, B. Scheiber, H. M. Sosik, M. Stephens, J. H. Swift. Massive phytoplankton
716 blooms under Arctic sea ice, *Science*. doi:10.1126/science.1215065.

717 Bates, N. R. and Mathis, J. T.: The Arctic Ocean marine carbon cycle: evaluation of air-sea
718 CO₂ exchanges, ocean acidification impacts and potential feedbacks, *Biogeosciences*, 6,
719 2433–2459, doi:10.5194/bg-6-2433-2009, 2009.

720 Bélanger S., J. Ehn, et M. Babin, (2007) Impact of sea ice on the retrieval of water-leaving
721 reflectance, chlorophyll a concentration and inherent optical properties from satellite Ocean
722 Color data, *Remote Sensing of Environment*, 111, 51-68.

723 Carmack, E. C. and Macdonald, W. R.: Oceanography of the Canadian Shelf of the Beaufort
724 Sea: A Setting for Marine Life, *Arctic*, 55, 29–45, 2002.

725 Dai A., Qian T., Trenberth K.E. and J. D. Milliman (2009) Changes in continental freshwater
726 discharge from 1949–2004. *Journal of Climate*, 22: 2773–2791.

727 Doxaran, D., Froidefond, J. M., Lavender, S. J., and Castaing, P.: Spectral signature of highly
728 turbid waters. Application with SPOT data to quantify suspended particulate matter
729 concentrations, *Remote Sens. Environ.*, 81, 149–161, 2002.

730 Doxaran, D., Froidefond, J. M., Castaing, P., and Babin, M.: Dynamics of the turbidity
731 maximum zone in a macrotidal estuary (the Gironde, France): Observations from field and

732 MODIS satellite data, *Estuar. Coast. Shelf Sc.*, 81, 321–332, 2009.

733 Doxaran, D., Ehn, J., Bélanger, S., Matsuoka, A., Hooker, S., and M. Babin (2012): Optical
734 characterisation of suspended particles in the Mackenzie River plume (Canadian Arctic
735 Ocean) and implications for ocean colour remote sensing, *Biogeosciences*, 9, 3213-3229,
736 doi:10.5194/bg-9-3213-2012.

737 Ehn J. K., Reynolds R. A., Stramski D., Doxaran D. and M. Babin. Forced variability in
738 suspended particulate matter patterns across the Canadian Beaufort Sea continental margin
739 (submitted to *Biogeosciences* Malina special issue).

740 Eisma, D., Bernard, P., Cade'e, G. C., Ittekkot, V., Kalf, J., Lanne, R., Martin, J. M., Mook,
741 W. G., Put, A., & Schuhmacher, T. (1991). Suspended matter particle size in some West-
742 European estuaries: Part II. A review on floc formation and break up. *Netherlands Journal of*
743 *Sea Research*, 28 (3), 215–220.

744 Emmerton, C. A., Lesack, L. F.W., and Vincent, W. F.: Nutrient and organic matter patterns
745 across the Mackenzie River, estuary and shelf during the seasonal recession of sea-ice, *J. Mar.*
746 *Syst.*, 74, 741–755, 2008.

747 Forest A., M. Babin, L. Stemann, M. Picheral, M. Sampei, L. Fortier, Y. Gratton, S.
748 Bélanger, E. Devred, J. Sahlin, D. Doxaran, F. Joux, E. Ortega-Retuerta, W.H. Jeffrey, J.
749 Martín, B. Gasser, J.C. Miquel, Ecosystem function and particle flux dynamics across the
750 Mackenzie Shelf (Beaufort Sea, Arctic Ocean): an integrative analysis of spatial variability
751 and biophysical forcings. *Biogeosciences*, 10, 2833-2866.

752 Franz B.A., Bailey S.W., Werdell P.J. and C. R. McClain, “Sensor independent approach to
753 the vicarious calibration of satellite ocean color radiometry,” *Appl. Opt.*, 46(22): 5068–5082,
754 2007.

755 Hedges, J. I., Keil, R. G., and Benner, R.: What happens to terrestrial organic matter in the
756 ocean?, *Org. Biogeochem.*, 27, 195– 212, 1997.

757 Keil R. G., Mayer L. M., Quay P. D., Richey J. E. and J. I. Hedges. Loss of organic matter
758 from riverine particles in deltas. *Geochimica et Cosmochimica Acta*, 61, 7, 1507-1511, 1997.

759 Markus, T. and D.J. Cavalieri, An enhancement of the NASA Team sea ice algorithm, *IEEE*
760 *Trans. Geoscience Remote Sensing*, 38, 1387-1398, 2000.

761 Macdonald, R.W., Solomon, S.M., Cranston, R.E., Welch, H.E., Yunker, M.B., Gobeil, C.,
762 1998. A sediment and organic carbon budget for the Canadian Beaufort Shelf. *Marine*
763 *Geology* 144, 255–273.

764 Macdonald, R.W., Harner, T., Fyfe, J., 2005. Recent climate change in the Arctic and its
765 impact on contaminant pathways and interpretation of temporal trend data. *Science of the*
766 *Total Environment* 342, 5–86.

767 McClelland J.W., Holmes R.M., Dunton K.H. and R. W. Macdonald. The Arctic Ocean
768 estuary. *Estuaries and Coasts*, 35: 353–368, 2012.

769 Meade, R.H., 1996. River-sediment inputs to major deltas. In: Milliman, J., Haq, B. (Eds.),
770 *Sea-Level Rise and Coastal Subsidence*. Kluwer, London, pp. 63–85.

771 Meister G., Franz B.A., Kwiatkowska E. J. and C.R. McClain. Corrections to the calibration
772 of MODIS Aqua ocean color bands derived from SeaWiFS data. *IEEE Transactions on*
773 *Geoscience and Remote Sensing*, 50(1): 310-319, 2012.

774 Nechad B., Ruddick K. & Park Y. (2010). Calibration and validation of a generic multisensor
775 algorithm for mapping of total suspended matter in turbid waters. *Remote Sensing of*
776 *Environment*, Vol. 114, pp. 854–866.

777 O'Brien, M. C., Macdonald, R. W., Melling, H., and Iseki, K.: Particle fluxes and
778 geochemistry on the Canadian Beaufort shelf: implications for sediment transport and
779 deposition, *Cont. Shelf Res.*, 26, 41–81, 2006.

780 Overland J., Bhatt U., Key J., Liu Y., Walsh J. and M. Wang (2011). Temperature and
781 Clouds. *Arctic Report Card: Update for 2011: Tracking recent environmental changes*.

782 http://www.arctic.noaa.gov/report11/temperature_clouds.html.

783 Perovich D., Gerland S., Hendricks S., Meier W., Nicolaus M., Richter-Menge J., Tschudi M.
784 (2013). Sea ice. Arctic Report Card: Update for 2013: Tracking recent environmental
785 changes. http://www.arctic.noaa.gov/reportcard/sea_ice.html.

786 Price D.T., R.I. Alfaro, K.J. Brown, M.D. Flannigan, R.A. Fleming, E.H. Hogg, M.P.
787 Girardin, T. Lakusta, M. Johnston, D.W. McKenney, J.H. Pedlar, T. Stratton, R.N. Sturrock,
788 I.D. Thompson, J.A. Trofymow, L.A. Venier. Anticipating the consequences of climate
789 change for Canada's boreal forest ecosystems. *Environmental Reviews*, 2013, 21(4): 322-365,
790 10.1139/er-2013-0042.

791 Rawlins, M.A., C.J. Willmott, A. Shiklomanov, E. Linder, S. Frolking, R.B. Lammers, and
792 C.J. Vörösmarty. 2006. Evaluation of trends in derived snowfall and rainfall across Eurasia
793 and linkages with discharge to the Arctic Ocean. *Geophysical Research Letters*, 33,
794 10.1029/2005GL025231.

795 Rontani J.F., Charriere B., Sempéré R., Doxaran D., Vaultier F., Vonk J.E. and J.K. Volkman
796 (2014). Degradation of sterols and terrestrial organic matter in waters of the Mackenzie Shelf,
797 Canadian Arctic. *Organic Geochemistry*, 75, 61–73.

798 Serreze, M.C., Walsh, J.E., Chapin, F.S.I., Osterkamp, T., Dyurgerov, M., Romanovsky, V.,
799 Oechel, W.C., Morison, J., Zhang, T., Barry, R.G., 2000. Observational evidence of recent
800 change in the northern high-latitude environment. *Climatic Change* 46, 159–207.

801 Smith C., Sheng Y., MacDonald G.M. and L. D. Hinzman (2005). Disappearing Arctic Lakes.
802 *Science*, 308(5727), 1429, DOI: 10.1126/science.1108142.

803 Shen, F., Salama, S., Zhou, Y., Jiufa Li, Zhongbo(Bob) Su and Dingbo Kuang. Remote-
804 sensing reflectance characteristics of highly turbid estuarine waters – a comparative
805 experiment of the Yangtze River and the Yellow River. *Int. J. of Remote Sensing*. 2010,
806 31(10):2639–2654.

807 Shiklomanov, A. I., R. B. Lammers, M. A. Rawlins, L. C. Smith, and T. M. Pavelsky, (2007),
808 Temporal and spatial variations in maximum river discharge from a new Russian data set, J.
809 Geophys. Res, 112, G04S53, doi:10.1029/2006JG000352.

810 Shiklomanov A. I. and R. B. Lammers (2011). River Discharge. Arctic Report Card: Update
811 for 2011: Tracking recent environmental changes.
812 http://www.arctic.noaa.gov/report11/river_discharge.html.

813 Syvitski (2002). Sediment discharge variability in Arctic Rivers: implications for a warmer
814 future. Polar Research, 21, 323-330.

815 Tremblay, J.-É., S. Bélanger, D.G. Barber, M. Asplin, J. Martin, G. Darnis, L. Fortier, Y.
816 Gratton, H. Link, P. Archambault, A. Sallon, C. Michel, W.J. Williams, B. Philippe, and M.
817 Gosselin, 2011. Climate forcing multiplies biological productivity in the coastal Arctic Ocean.
818 Geophys. Res. Lett. 38, L18604, doi:10.1029/2011GL048825.

819 Trenberth K. E. (2011). Changes in precipitation with climate change. Climate Research, 47:
820 123-138.

821 Wang, M. and Shi, W.: The NIR-SWIR combined atmospheric correction approach for
822 MODIS ocean color data processing, Opt. Express, 15, 15722–15733, 2007.

823 Wissler, D., B. M. Fekete, C. J. Vörösmarty, and A. H. Schumann (2010): Reconstructing 20th
824 century global hydrography: a contribution to the Global Terrestrial Network- Hydrology
825 (GTN-H), Hydrology and Earth System Science, 14, 1-24.

826 Yunker, M. B., Macdonald, R.W., Cretney, W. J., Fowler, B. R., and F. A. McLaughlin:
827 Alkane, terpene, and polycyclic aromatic hydrocarbon geochemistry of the Mackenzie River
828 and shelf: riverine contributions to Beaufort Sea coastal sediments, Geochim. Cosmochim.
829 Ac., 57, 3041–3061, 1993.

830 Zhang Y., Li J., Wang X., Chen W., Sladen W., Dyke L., Dredge L., Poitevin J., McLennan
831 D., Stewart H., Kowalchuk S., Wu W., Kershaw G. P. and R. K. Brook: Modelling and

- 832 mapping permafrost at high spatial resolution in Wapusk National Park, Hudson Bay
- 833 Lowlands. *Canadian Journal of Earth Sciences*, 2012, 49: 925-937, 10.1139/e2012-031.
- 834

835 **Figure legends**

836

837 **Figure 1.** Variations of air temperature and precipitation anomalies observed in the
838 Mackenzie drainage basin from 1973 to 2013 (a). Variations of the Mackenzie freshwater
839 discharge (monthly and yearly averages); trends observed between 1973 and 2013, and
840 between 2003 and 2013 (b). Zoom on the variations of the Mackenzie freshwater discharge
841 between 2003 and 2013 (c).

842

843 **Figure 2.** Quasi-true colour MODIS-Aqua image recorded on 24 June 2004 (250 m spatial
844 resolution). The study area includes the: (i) Mackenzie River mouth West and East branches
845 (red box) and delta zone (green box) and (ii) the Beaufort Sea in the Canadian Arctic Ocean.
846 During winter time the connection between the river delta and adjacent coastal waters is
847 closed by the stamukha while drifting sea-ice develops offshore.

848

849 **Figure 3.** Example of processing (atmospheric corrections to retrieve the remote sensing
850 reflectances at 555 and 748 nm then inversion of the 748:555 reflectance band ratio into SPM
851 concentration) applied to L1B MODIS-Aqua data on 4 July 2007: a) NIR-SWIR atmospheric
852 correction with default mask thresholds; b) NIR-SWIR atmospheric correction with cloud-
853 albedo threshold set to 0.4 (instead of 0.027) in the river delta zone; c) merged product.

854

855 **Figure 4.** Number of L2 images available for each month of the time series (images selected
856 after visual inspection).

857

858 **Figure 5.** Typical SPM and sea-ice concentrations (in g m^{-3} and %, respectively) maps
859 obtained over the study area in selected days in June, July and August 2004. From June to

860 July the breaking of the stamukha results in the discharge of turbid freshwater from the
861 Mackenzie River into the Beaufort Sea. Even during the summer period the delta zone
862 remains the most turbid area (maximal SPM concentrations).

863

864 **Figure 6.** Monthly (June to September) composites of sea-ice and surface water SPM
865 concentrations in 2003 and 2004.

866

867 **Figure 7.** Same as Figure 6 in 2006 and 2008.

868

869 **Figure 8.** Same as Figure 6 in 2011, 2012 and 2013.

870

871 **Figure 9.** Multi-year (2003-2013) variations and trend of the monthly-averaged SPM
872 concentration at the Mackenzie River mouth (a). Plot of the monthly-averaged SPM
873 concentration as a function of the monthly-averaged freshwater discharge: considering all
874 months (white circles) then only considering the months of May and June (red circles) (b).
875 The determination coefficients (R^2) correspond to the best linear fits.

876

877 **Figure 10.** Monthly-averaged SPM flux (in g) estimated at the river mouth (geographical
878 zone defined as a box: $68.7^\circ\text{N} - 69.5^\circ\text{N}$ and $133^\circ\text{W} - 137^\circ\text{W}$) in June, July, August and
879 September, from 2003 to 2013 (a). Same in the delta zone (geographical zone defined as a
880 box: $68.7^\circ\text{N} - 70^\circ\text{N}$ and $132^\circ\text{W} - 139^\circ\text{W}$) (b). Total estimated mass (in g) of SPM delivered
881 by the Mackenzie River into the Beaufort Sea during the summer period (June to September)
882 from 2003 to 2013 (c). The best-fitted linear trend is overplotted.

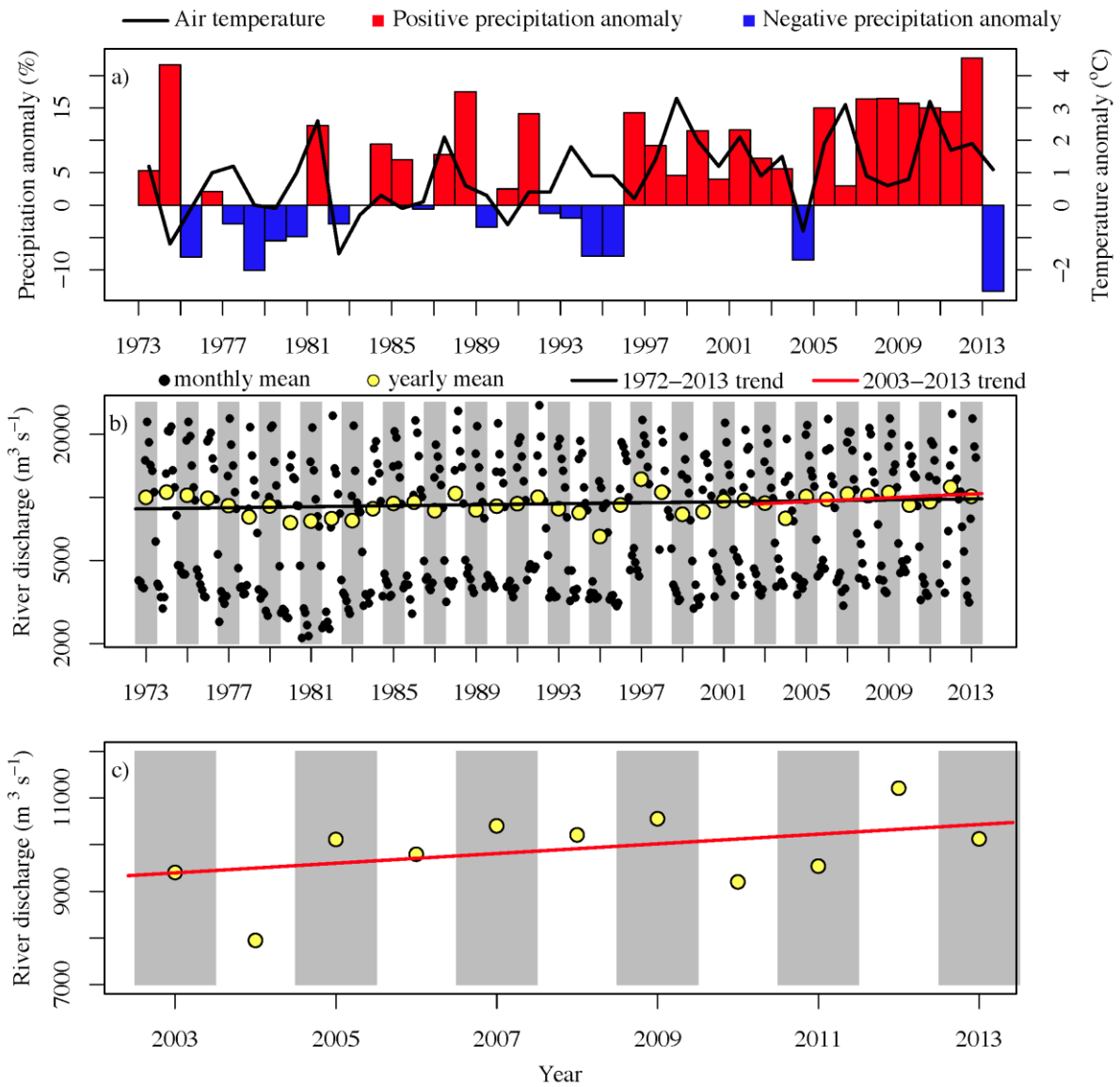
883

884 **Figure 11.** Multi-year (2003-2013) trends in the variation of the monthly-averaged SPM

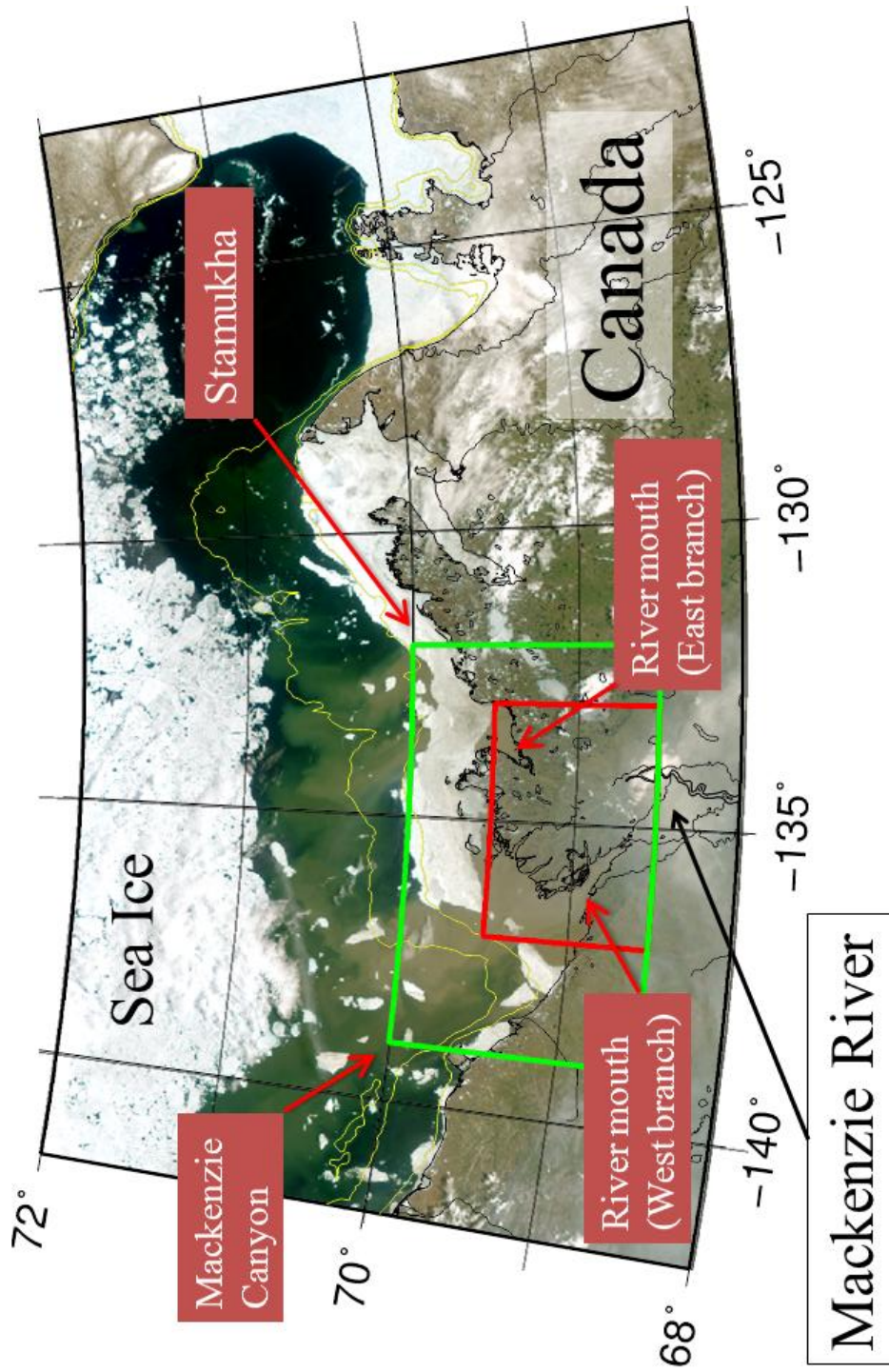
885 concentration over the Mackenzie River plume (a) and extent of the river plume (b).

886

887 **Figures**
888

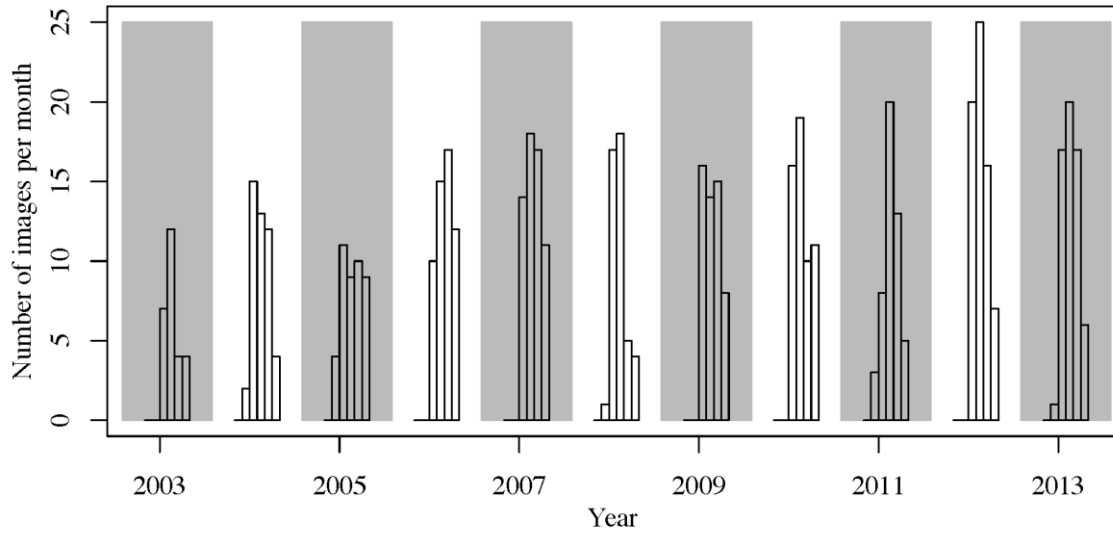


889
890
891 **Figure 1**
892
893



894
 895
 896
 897

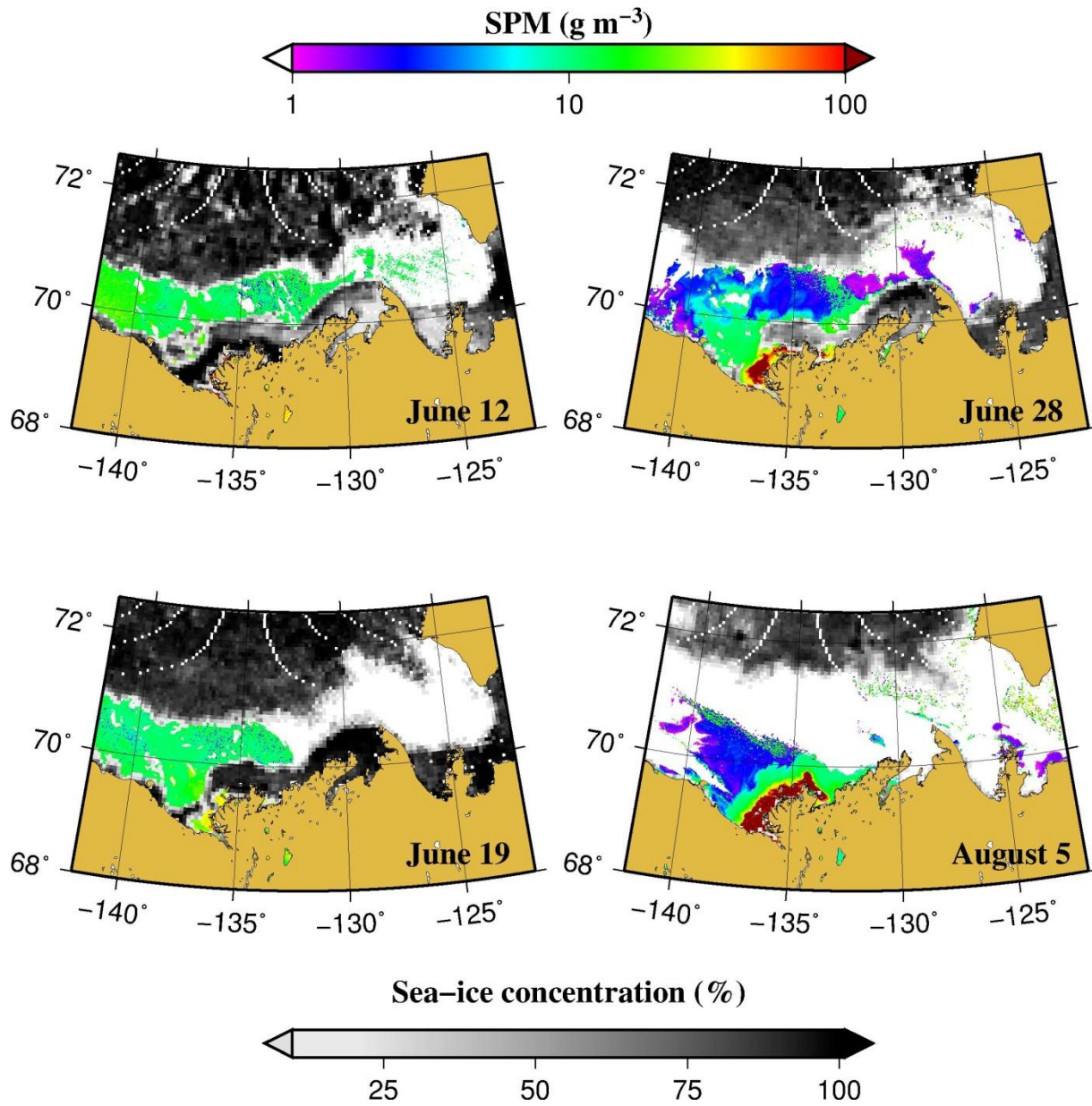
Figure 2



903
 904
 905
 906
 907

Figure 4

908
909
910
911
912
913

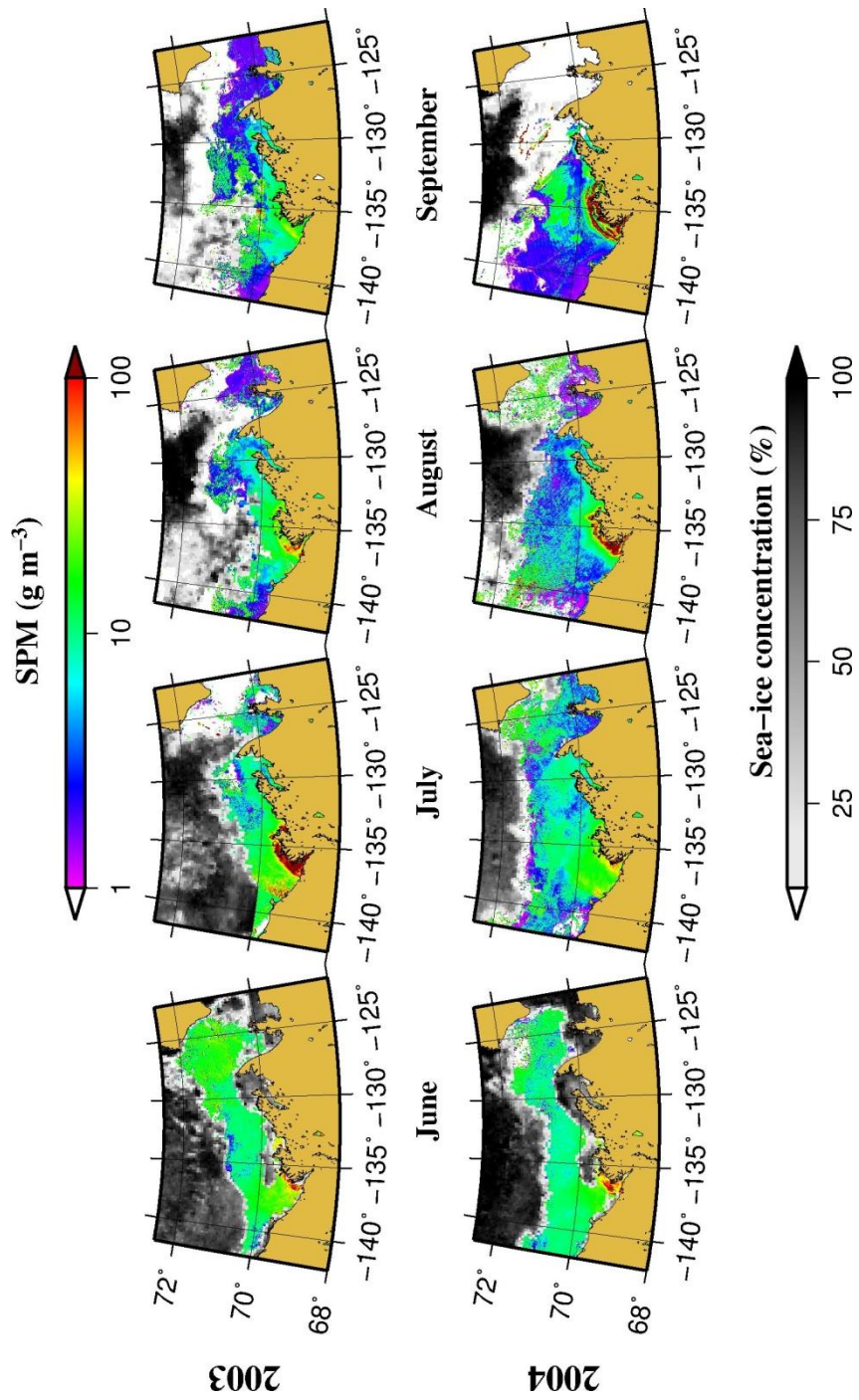


914
915
916
917
918

Figure 5

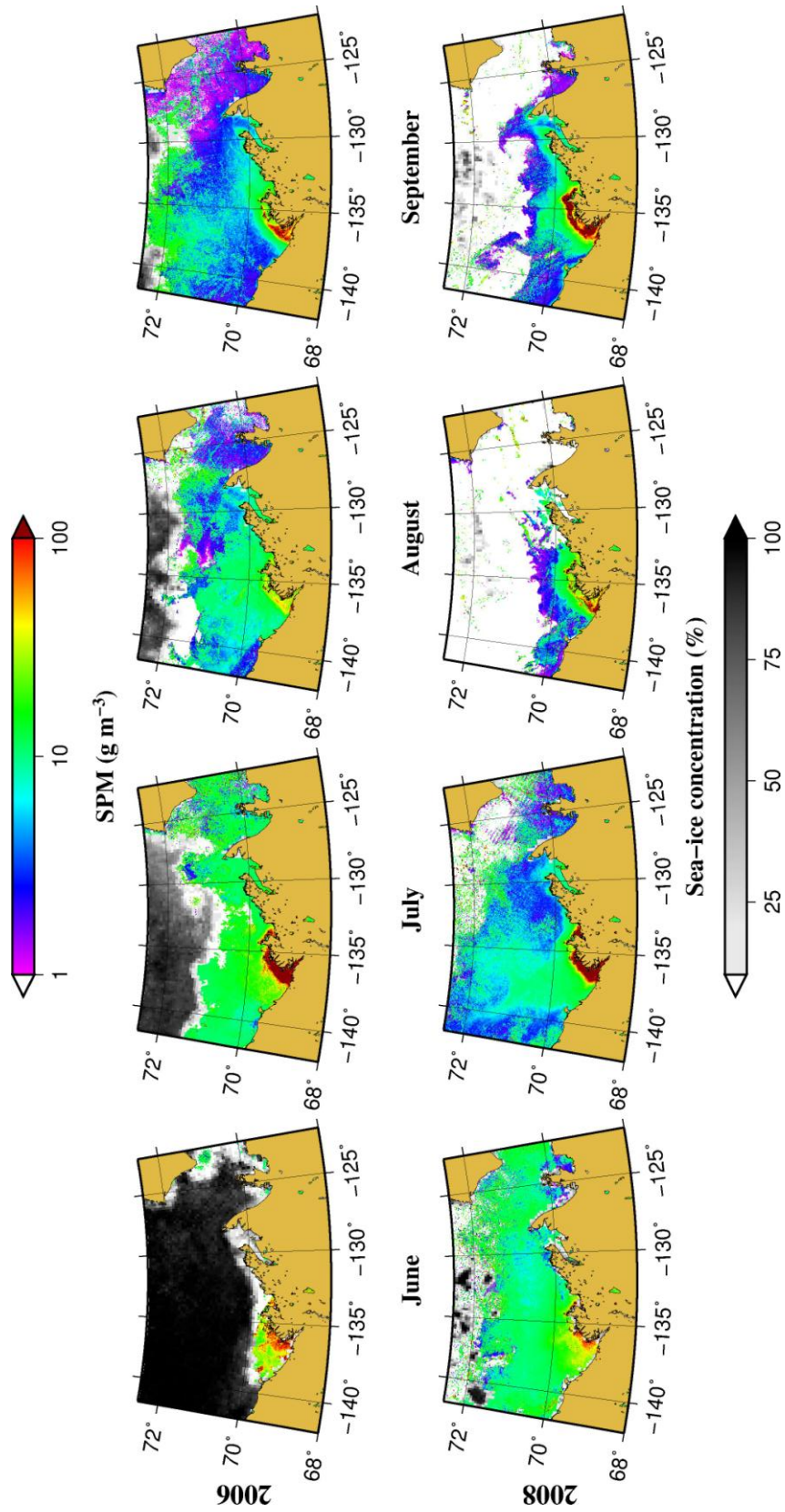
919
920
921
922
923

Figure 9



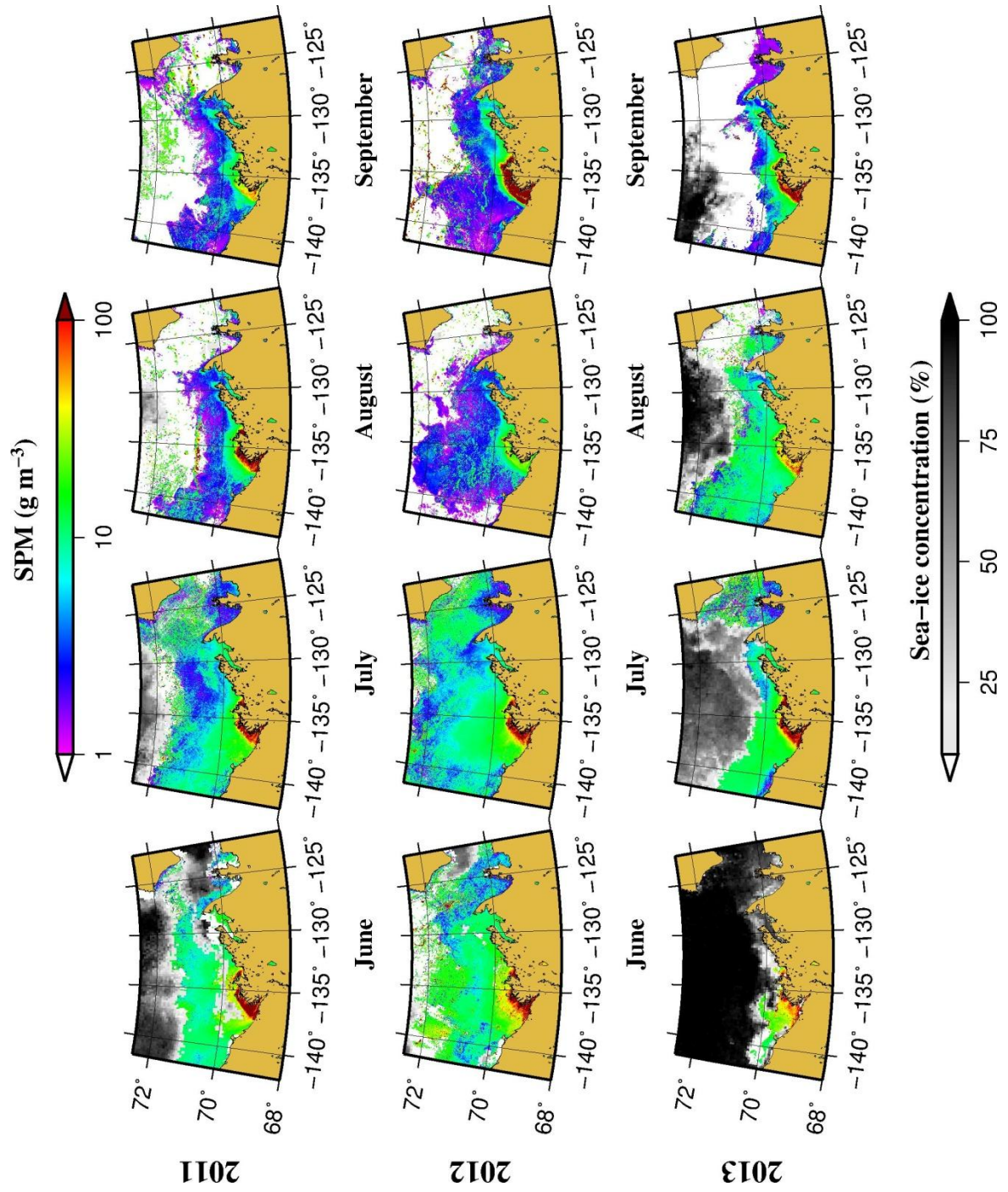
924
925
926
927

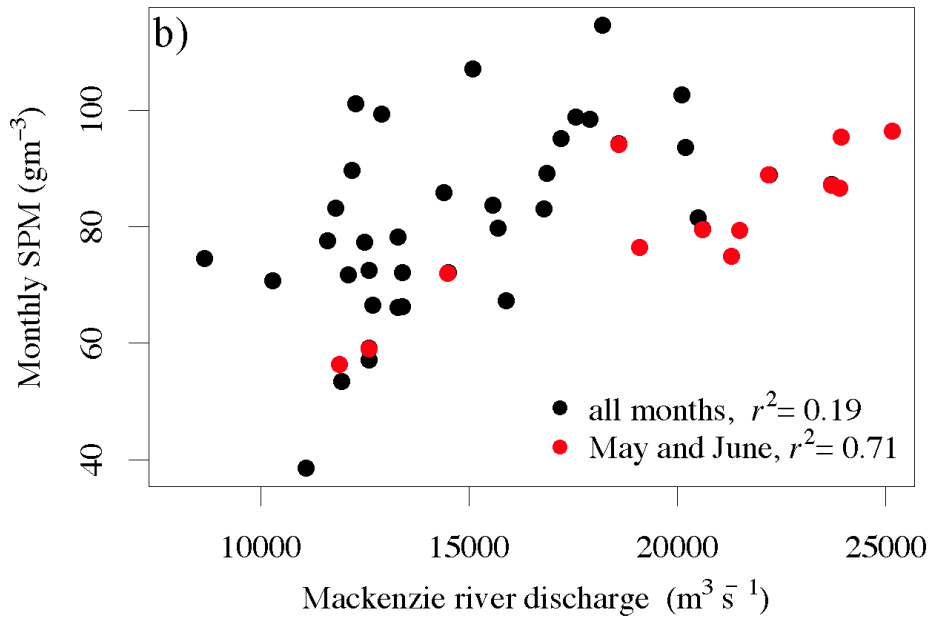
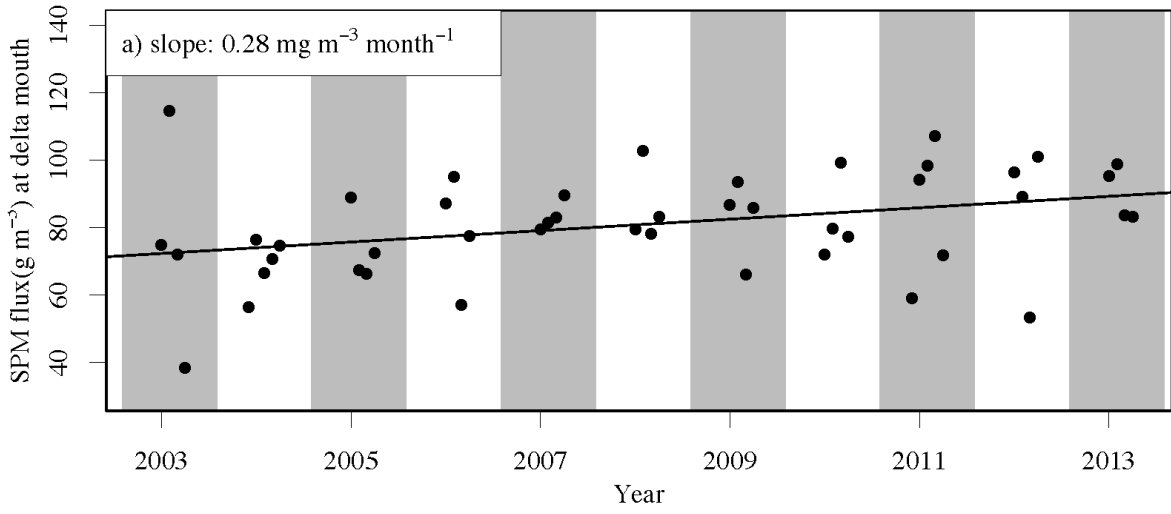
Figure 7



928
929
930

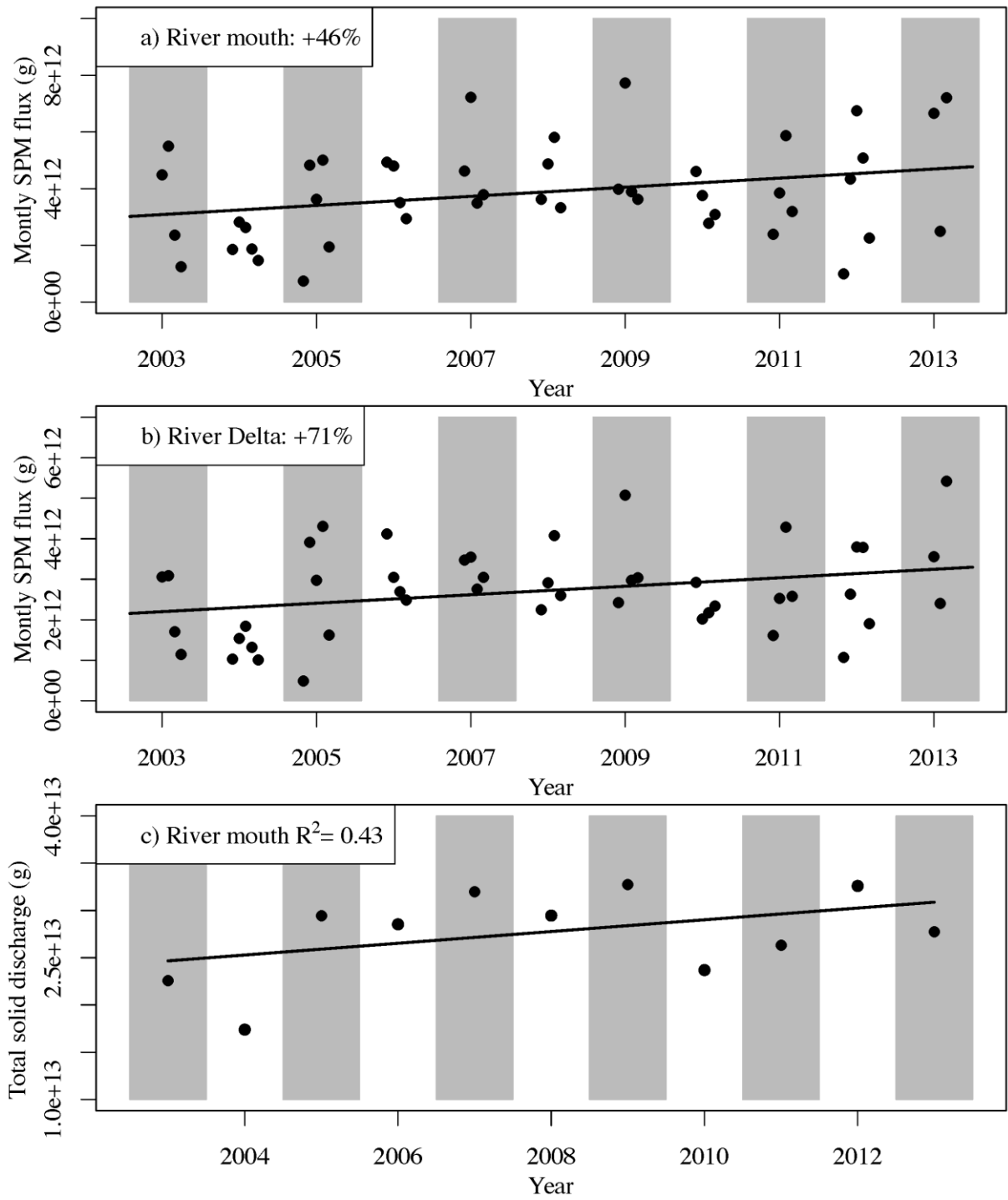
Figure 8





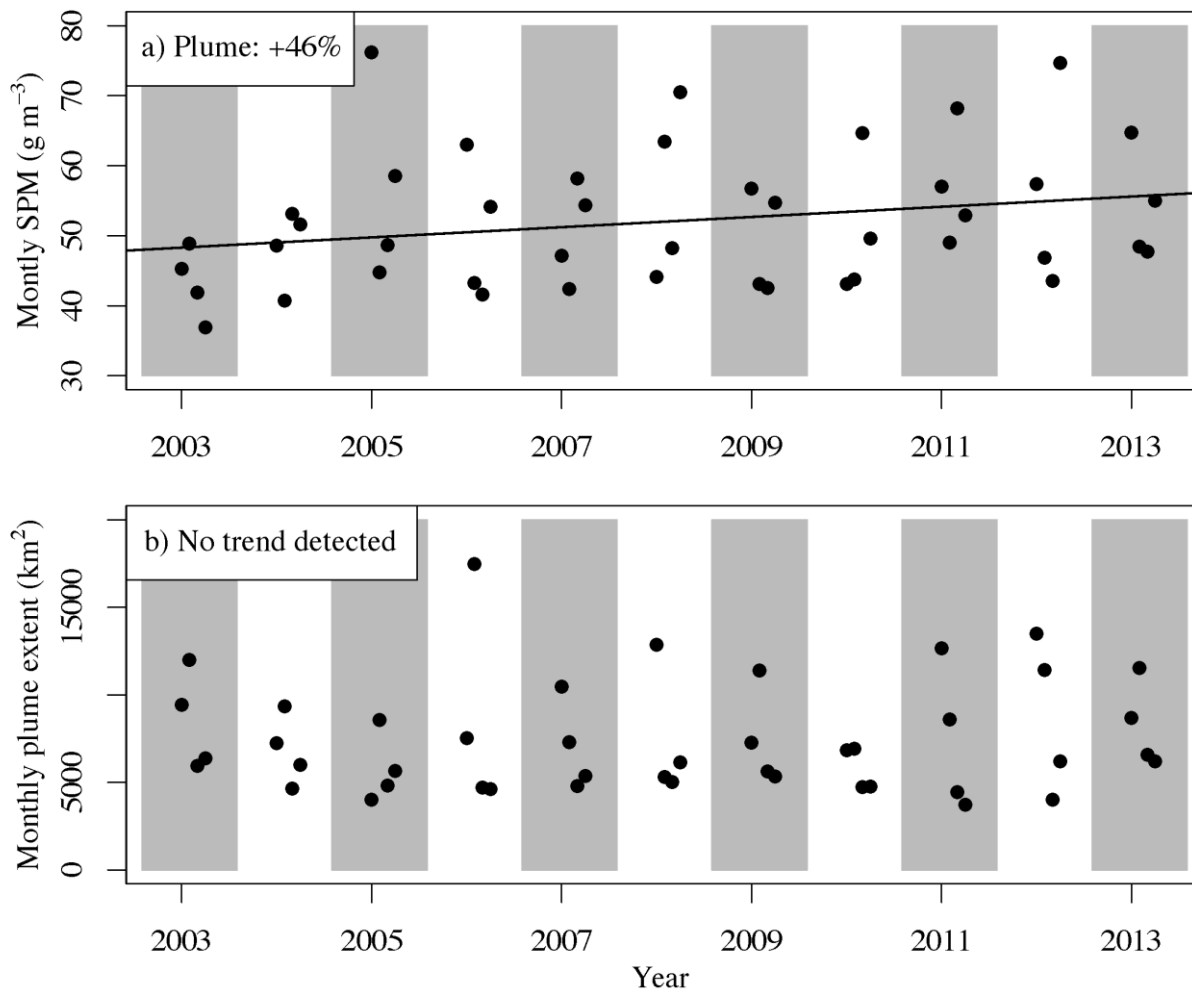
931
 932
 933
 934
 935
 936
 937
 938
 939
 940

Figure 9



941
 942
 943
 944
 945

Figure 10



946
 947
 948
 949

Figure 11